Opposite Trends in the Northern Hemisphere Stratosphere Between Mid-Winter and Early Spring Linked to Surface Temperature Anomalies

Gwendal Rivière, Fabio D'Andrea, Daniela Domeisen, Alice Portal

Geophysical Research Letters

RESEARCH LETTER
10.1029/2024GL109746

Opposite Trends in the Northern Hemisphere Stratosphere Between Mid-Winter and Early Spring Linked to Surface Temperature Anomalies

Gwendal Rivière[1], Fabio D'Andrea[1], Daniela I. V. Domeisen[2,3], and Alice Portal[4]

[1]LMD-IPSL, École Normale Supérieure, PSL Research University, Sorbonne Université, École Polytechnique, IP Paris, CNRS, Paris, France, [2]Institute of Earth Surface Dynamics, Université de Lausanne, Lausanne, Switzerland, [3]Institute for Atmospheric and Climate Science, Zurich, Switzerland, [4]Institute of Geography, Oeschger Centre for Climate Change Research, University of Bern, Bern, Switzerland

Abstract Trends in the coupled stratosphere-troposphere system during the 1979–2022 period are investigated in the Northern Hemisphere using reanalysis datasets. More upward planetary wave propagation in December is shown to precede the deceleration of the stratospheric polar vortex in January. This deceleration prevents the waves from continuing to propagate upward in February and favors an acceleration of the stratospheric polar vortex in March. This is associated with an increased Northern Hemisphere annular mode in March in the stratosphere and the troposphere. Trends show a moderate significance level because of strong interannual variability. Recent seasons whose anomalies project onto the trends are those for which wave-1 anomaly constructively interferes with wave-1 climatology in December, which occurs when there is warming in an area extending from Eastern Canada to Greenland and slight cooling over Eurasia. It shows the potential for predicting the springtime stratospheric polar vortex from wintertime wave-1 anomalies.

Plain Language Summary In winter the stratosphere hosts strong westerly winds forming the stratospheric polar vortex. Variations in the vortex strength can affect weather patterns in the underlying troposphere. Vice-versa, the stratospheric vortex can also be disrupted by tropospheric waves that propagate upwards into the stratosphere. Sea-ice loss from Arctic warming is amongst the forcings that have been proposed to produce tropospheric waves leading to a weakening of the polar vortex. However, there is a strong dependence of the stratospheric signal on the region of sea ice loss. In the present study, we show that mid-winter to early spring stratospheric trends during the 1979–2022 period are linked to large-scale surface temperature trends in December. Specifically, strong warming from Eastern Canada to Greenland and relative cooling over Eurasia in December are associated with enhanced upward wave propagation and a deceleration of the stratospheric polar vortex in January. In mid-winter a weaker than usual vortex inhibits wave propagation to the stratosphere, allowing for a recovery in vortex strength by March. In conclusion, our work shows how the opposite mid-winter and early spring trends in the stratosphere can be connected with stronger wave propagation from the surface in December and with its time-evolving effects on troposphere–stratosphere coupling.

Key Points:

- January and March exhibit opposite trends in the stratospheric Northern Annular Mode (NAM) during 1979–2022
- The negative (positive) trend in the NAM in January (March) is explained by more (less) upward wave propagation in December (February)
- More upward wave propagation in December is linked to warming over Eastern Canada and cooling over Siberia

Supporting Information:

Supporting Information may be found in the online version of this article.

Correspondence to:

G. Rivière,
griviere@lmd.ens.fr

Citation:

Rivière, G., D'Andrea, F., Domeisen, D. I. V., & Portal, A. (2024). Opposite trends in the Northern Hemisphere stratosphere between mid-winter and early spring linked to surface temperature anomalies. *Geophysical Research Letters*, *51*, e2024GL109746. https://doi.org/10.1029/2024GL109746

Received 12 APR 2024
Accepted 2 SEP 2024

Author Contributions:

Conceptualization: Gwendal Rivière, Fabio D'Andrea, Daniela I. V. Domeisen, Alice Portal
Formal analysis: Gwendal Rivière
Methodology: Gwendal Rivière
Validation: Gwendal Rivière, Fabio D'Andrea, Daniela I. V. Domeisen, Alice Portal
Writing – original draft: Gwendal Rivière, Fabio D'Andrea, Daniela I. V. Domeisen, Alice Portal

1. Introduction

The changes in the stratospheric polar vortex (SPV) during recent decades have received a lot of attention because of the vortex' role in stratosphere-troposphere interactions and its potential impacts on mid-latitude weather. Several studies detected a weakening of the wintertime polar vortex and a shift toward lower latitudes (Seviour, 2017; Zhang et al., 2016). A possible cause for such changes is the fast Arctic warming, known as the Arctic Amplification and its associated reduction in Arctic sea ice, but this mechanism is still strongly debated (Cohen et al., 2020; Liang et al., 2023; Peings et al., 2023; Peings, 2019; L. Sun, Deser, et al., 2022). The usually invoked mechanism is the following: Arctic sea ice loss, which is most pronounced over the Barents-Kara seas region, favors the formation of a Siberian high anomaly and upward propagating waves. More upward propagating waves decelerate the stratospheric polar vortex that then in turn influences the troposphere by favoring the negative phase of the Northern Annular Mode (NAM) and of the North Atlantic Oscillation (e.g., Hoshi et al., 2019; Kim et al., 2014; Kretschmer et al., 2020).

Numerical experiments only partly confirm the above mechanistic arguments deduced from observations. The large variety of numerical modeling responses to Arctic sea-ice loss is likely linked to the different model setups

in terms of sea ice reduction and Arctic warming and to the compensating effects of various warming patterns over different Arctic regions (L. Sun et al., 2015; Screen, 2017). It is mainly the warming over the Barents-Kara seas region that leads to a weakening of the stratospheric polar vortex during mid-winter (Ruggieri et al., 2017; Screen, 2017). Usually, the response of the SPV to sea ice loss in numerical modeling experiments is weak compared to internal variability and a large ensemble of simulations is needed to obtain a significant signal (Seviour, 2017; L. Sun, Deser, et al., 2022). Similarly, the response of the SPV to increased CO_2 is uncertain and strongly model dependent, mostly due to model biases in the lower stratosphere (Karpechko et al., 2024). The highest model uncertainty is found in winter, with impacts on surface climate (Karpechko et al., 2022), but with a signal toward a longer seasonal duration of the SPV (Ayarzagüena et al., 2020).

While most of the literature focuses on the wintertime SPV, several studies have investigated the impacts of winter Arctic sea ice decline on the tropospheric and stratospheric circulations in spring. By performing numerical experiments using a coupled chemistry climate model with a well-resolved stratosphere, L. Sun et al. (2014) and L. Sun et al. (2015) showed that the projected sea ice loss creates a deceleration of the SPV in winter and an acceleration of the SPV in spring accompanied by ozone depletion. More recently, using reanalysis data, J. Sun, Liu, et al. (2022) found a strong correlation during the 2001–2018 period between sea ice anomalies in winter over the Barents-Kara sea regions and Eurasian extreme heat events in spring. Here again, the stratospheric pathway was shown to be the key to understand this link.

The present paper aims at revisiting trends in the coupled troposphere-stratosphere system from winter to spring using the most recent years of reanalysis data. This study is motivated by the fact that previous studies showing trends focused on winter only and on a shorter period of time (Cohen et al., 2014; Hu et al., 2018, 2019). Here we consider the satellite era (1979–2022) because stratosphere-troposphere coupling was shown to be consistently represented by recent reanalyzes from 1979 onwards (Gerber & Martineau, 2018; SPARC, 2022, see chapter 6) and because Arctic warming has strongly accelerated during the last two decades of this period. However, caution should be taken in the analysis of reanalysis temperature trends during that period too due to changes in observational systems (Long et al., 2017; SPARC, 2022, see chapter 3).

2. Data and Method

The paper relies on daily and monthly means of ERA5 reanalysis from 1979 to 2022 (Hersbach et al., 2020). The horizontal grid resolution is 0.75° and vertical levels are located at 10, 20, 30, 50, 70 hPa and every 100 hPa from 100 hPa to 1000 hPa. For comparison, two supplementary figures (Figures S1 and S2 in Supporting Information S1) also use monthly means of Modern-Era Retrospective Analysis for Research and Applications (MERRA-2) from 1980 to 2022 (Gelaro et al., 2017).

The Northern Annular Mode (NAM) is defined for each individual month as the first EOF (EOF1) of the zonal and monthly mean geopotential height from 20°N to 90°N at each pressure level separately. The monthly NAM index is the first principal component (PC1) associated with EOF1. The positive phase is defined as averaged geopotential anomalies larger in mid-latitude than polar regions, across levels and seasons. The daily NAM index is defined as the normalized projection of the daily geopotential height anomaly onto EOF1 of the corresponding month.

The trends correspond to least squares linear regression estimates and their statistical significance is based on the test of Santer et al. (2000) with N-2 degrees of freedom where $N = 44$ years for the 1979–2022 period. Statistical significance of Pearson correlation coefficients relies on the assumption of a t distribution with N-2 degrees of freedom where N is the number of years ($N = 44$ for the 1979–2022 period and $N = 22$ for the 1979–2000 or 2001–2022 periods).

The vertical component of the Eliassen-Palm fluxes, which in the quasi-geostrophic framework is proportional to heat fluxes, is expressed in pressure coordinates (Edmon et al., 1980):

$$F_p = fa\cos\varphi[v^*\theta^*]/[\theta_p], \quad (1)$$

where f is the Coriolis parameter, a the Earth's radius, φ the latitude, v the meridional wind, θ the potential temperature and θ_p the pressure derivative of θ. The parentheses [.] and superscripts $.^*$ denote the zonal mean and the deviations from the zonal mean, respectively.

The decomposition of the heat fluxes into a linear and nonlinear component has been shown to be useful to better understand processes at play in the upward wave propagation (Fletcher & Kushner, 2011; Smith & Kushner, 2012). The meridional wind and potential temperature deviations from zonal mean are separated into a stationary wave component and a transient wave component.

$$v^* = \overline{v^*} + v^{*\prime}, \tag{2}$$

$$\theta^* = \overline{\theta^*} + \theta^{*\prime}, \tag{3}$$

where the overbar denotes the climatological mean and prime denotes the deviation from the climatological mean. It leads to

$$\begin{aligned}[v^*\theta^*]_{trend} &= \left[\overline{v^*}\theta^{*\prime}\right]_{trend} + \left[v^{*\prime}\overline{\theta^*}\right]_{trend} + \left[v^{*\prime}\theta^{*\prime}\right]_{trend} \\ &= \text{LIN} + \text{NL},\end{aligned} \tag{4}$$

where LIN and NL are the linear and nonlinear components.

$$\text{LIN} = \left[\overline{v^*}\theta^{*\prime}\right]_{trend} + \left[v^{*\prime}\overline{\theta^*}\right]_{trend}, \tag{5}$$

$$\text{NL} = \left[v^{*\prime}\theta^{*\prime}\right]_{trend}. \tag{6}$$

LIN corresponds to the interactions among stationary and transient waves, while NL corresponds to nonlinear interactions among the transient waves. Horizontal averages of various quantities are hereafter computed using a weighting by the cosine of latitude.

3. Results

ERA5 trends during 1979–2022 are shown in Figure 1 as a function of calendar month (see the equivalent figure for MERRA-2 in Figure S1 in Supporting Information S1). Three main areas of significant trends at the 95% confidence level are detected for both datasets. The first one is the Arctic warming in the lower troposphere present for all months throughout the year, with the strongest surface warming observed in October to February (Figure 1a), consistent with Cohen et al. (2020). The second significant trend is observed during the summer months from June to September in the lower stratosphere, characterized by a cooling between 100 hPa and 20 hPa (Figure 1a), a slight acceleration of the easterlies in the middle stratosphere (10–20 hPa) (Figure 1b) and a decrease in the stratospheric NAM (Figure 1c, see also the supporting information, in particular Figure S2 in Supporting Information S1 for further details on these trends). The third and strongest significant trend is in March, marked by a cooling up to −2.0 K per decade throughout the lower and middle stratosphere (Figure 1a), an acceleration of the mid-latitude westerlies in both the stratosphere and troposphere (Figure 1b) and a positive trend in the stratospheric and tropospheric NAM (Figure 1c). Opposite-signed trends occur in January as compared to March: the stratosphere warms, the mid-latitude westerlies decelerate and the NAM decreases. However, except at 10 hPa, January trends are not statistically significant at the 95% confidence level. This study is dedicated to better understand the differing trends between mid-winter and early spring.

To identify potential time lags between stratospheric and tropospheric trends, Figure 2 shows trends at daily time scales from December to April and between 1,000 hPa and 10 hPa. The warming trend of the stratosphere, the higher geopotential height values and the negative NAM trend in January reach the largest values in the middle stratosphere at 10 hPa (Figures 2a and 2b). January trends are preceded by positive trends in upward wave propagation of wavenumbers 1 and 2 between mid-December and early January, the one in early January being statistically significant at 99% (Figure 2c). The wave propagation trends start in the troposphere and reach the stratosphere with a time-lag on the order of a week. The trend toward a decelerated polar vortex and a decreased stratospheric NAM in January is only weakly significant and no significant impact in the troposphere is detected. In mid-February, trends in Arctic temperature, Arctic geopotential height, NAM and mid-latitude zonal wind change sign in the stratosphere, simultaneously with strong negative trends in upward propagating waves (Figures 2a–2c). Between mid-February and mid-March, Arctic cooling and negative geopotential trends develop

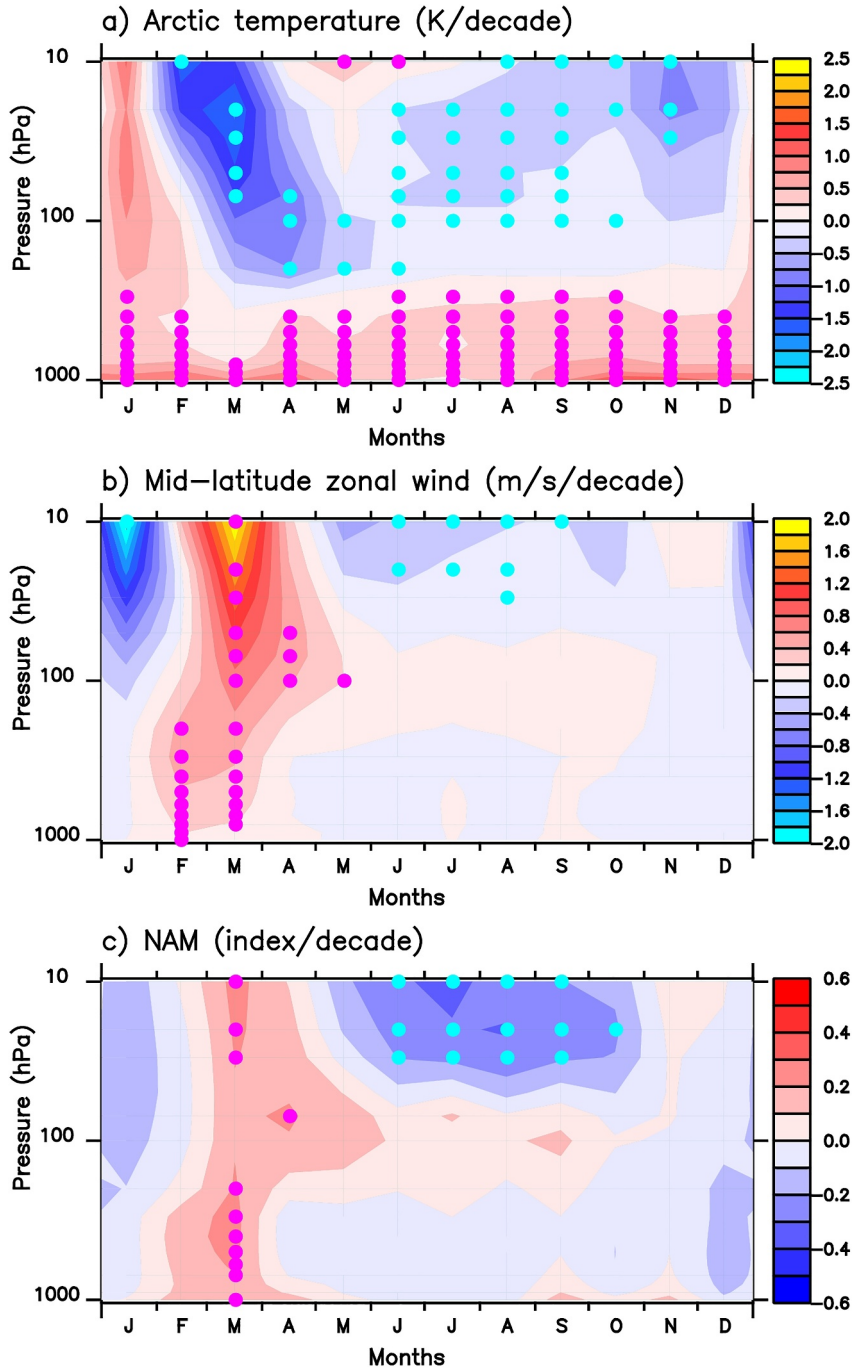

Figure 1. Trends from 1979 to 2022 as a function of the months of (a) zonally and latitudinally (70°N-90°N) averaged temperature (units: K per decade), (b) zonally and latitudinally (40°N-70°N) averaged zonal wind (units: m s^{-1} per decade) and (c) Northern Annular Mode (units: normalized index per decade). Red and blue dots correspond to statistically significant positive and negative trends, respectively, at the 95% confidence level (one-tailed test). Data: ERA5 reanalysis at monthly resolution.

in the lower stratosphere together with a positive NAM trend. In mid-March, the positive NAM trend is statistically significant at 95% throughout the vertical column with normalized NAM index trend values reaching 0.3 per decade. The downward propagation signal of the NAM trend in February-March is reminiscent of the composites of strong polar vortex events (Baldwin & Dunkerton, 2001; Gerber & Martineau, 2018).

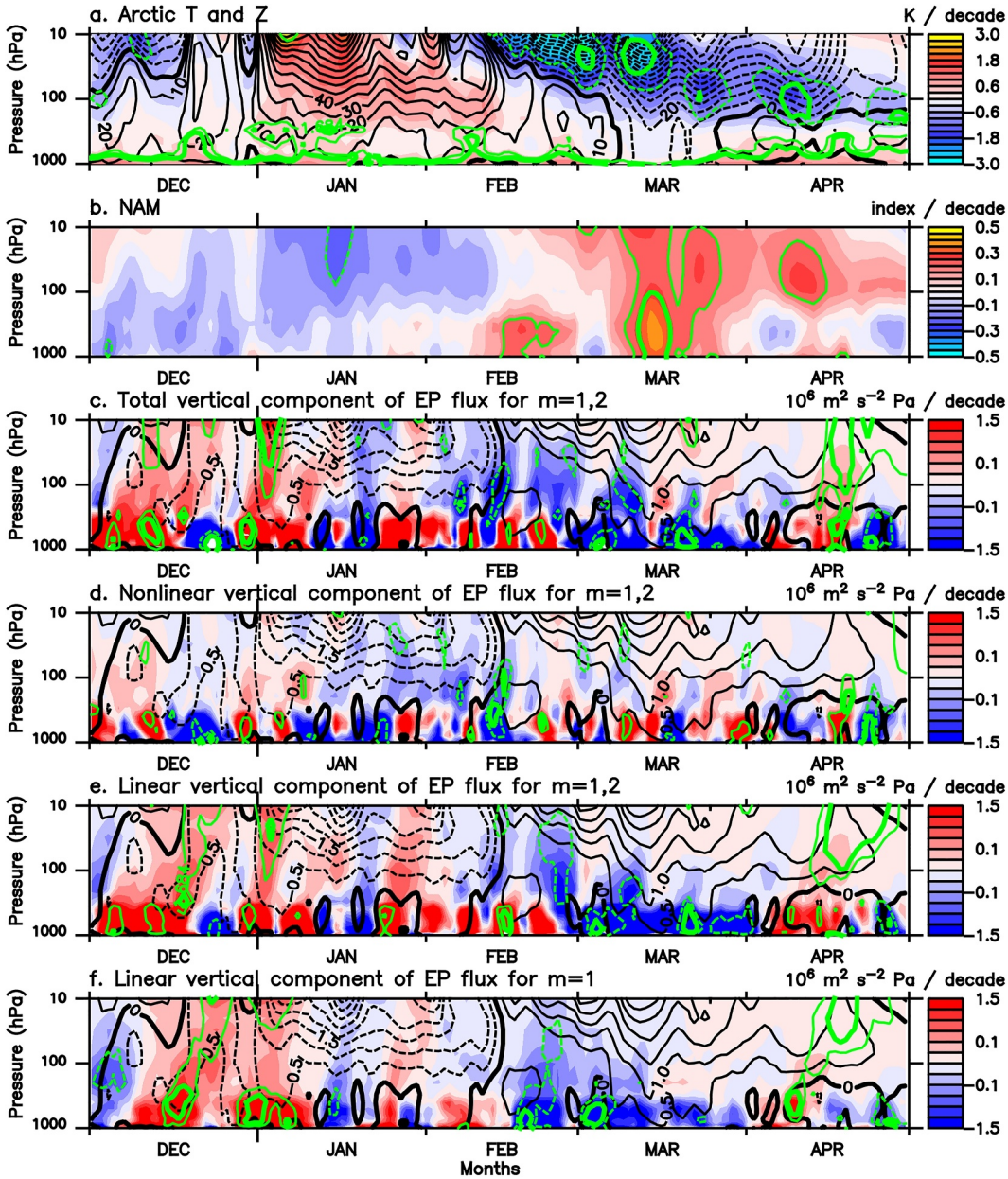

Figure 2. Trends from 1979 to 2022 between December and April of (a) polar cap zonally and latitudinally (70°N-90°N) averaged temperature (shading, units: K per decade) and geopotential height (contours: 10 m per decade), (b) Northern Annular Mode (units: normalized index per decade), (c) latitudinally (50°N-70°N) averaged total vertical component of EP flux F_p for zonal wavenumbers $m = 1, 2$ (units: $10^6 m^2\ s^{-2}$ Pa per decade), (d) nonlinear vertical component of EP flux (NL, see Equation 6) for $m = 1, 2$, (e) linear vertical component of EP flux (LIN, see Equation 5) for $m = 1, 2$ and (f) linear vertical component of EP flux (LIN, see Equation 5) for $m = 1$. Black contours in panels (c) to (f) show the latitudinally (50°N-70°N) averaged zonal wind trend (interval: 0.5 m s^{-1} per decade). Thin and bold green contours correspond to statistically significant patterns at the 95% and 99% level (one-tailed test), respectively. Data: ERA5 at daily time scales.

The following chain of events is suggested by the results in Figures 2a–2c. Increased upward wave propagation in late December leads to a deceleration of the stratospheric polar vortex in January. Such a deceleration of the westerlies reduces or even prevents upward wave propagation, which in turn helps to restore the stratospheric polar vortex by radiative cooling, inducing a positive NAM in the stratosphere and subsequently in the troposphere in early spring. This mechanism shows similarities with the one described in Rupp et al. (2023).

While the linear trend is significant, large interannual variability is present and not all winters show this chain of events. As an example we show an analysis of the seven recent winters from 2015 to 2022 (Figures S3, S4 and S5

in Supporting Information S1). Only two winters (2018–2019, 2020–2021) follow the scenario suggested by the trend patterns. These two winters are characterized by sudden stratospheric warmings in early January. Two other winters follow the opposite scenario with late stratospheric warmings in early March (2015–2016 and 2021–2022). The other three winters (2016–2017, 2017–2018 and 2019–2020) do not show a clear relationship with the trends. For instance, winter 2019–2020 exhibits a strong positive NAM phase all the way from early January to mid-April (Figure S4 in Supporting Information S1). By removing winter 2019–2020 from the computation, the NAM trend in March becomes weaker and less significant (at 90% confidence level), whereas the negative trend in January grows stronger, making the opposite trends in January and March more symmetric (not shown).

To highlight interferences of trends with climatological waves, Figures 2c-2e show the total, NL and LIN components of F_p, respectively, for wavenumbers 1 and 2 (Equation 4). The positive trend in F_p in January is mainly explained by the linear component. The negative trend in February is also mainly due to the linear trend, with the weaker nonlinear trend reinforcing the linear one. The linear trend for wavenumber 1 dominates that for wavenumbers 1 and 2 (compare Figures 2e and 2f). Specifically, wavenumber 1 shows more upward wave propagation between mid-December and early January and less upward wave propagation between mid-February and early March. These results mean that the linear interference of wave-1 trend with wave-1 climatology explains the largest part of the trend in heat fluxes.

Constructive interference of the wave-1 trend with wave-1 climatology in December is obvious over the whole atmospheric column in Figures 3e–3i and 3m. Near the surface it corresponds to a positive temperature trend along a sector extending from Eastern Canada to the Barents-Kara sea, where the climatological wave-1 temperature signal is positive, and a negative temperature trend from Central Siberia to Alaska, where the climatological wave-1 temperature signal is negative. This pattern is associated with a significant warming trend over Eastern Canada, the Hudson Bay and the Labrador sea and over the Barents-Kara seas region (Figure 3a). The weak and not significant negative temperature trend over Siberia is reminiscent of the Warm Arctic-Cold continent pattern (Overland et al., 2011; L. Sun et al., 2016).

In January, the wave-1 constructive interference diminishes mainly because the warming trend over eastern Canada is reduced compared to December (Figures 3b–3f and 3j), even though the eddy heat flux is still positive on average (Figure 3n). In February, the wave-1 trend and the wave-1 climatology destructively interfere as there is no more warming trend over Eastern Canada and instead Eurasia tends to warm (Figures 3c–3g, 3k and 3o). The Eurasian warming is even more pronounced in March (Figures 3d–3h, 3l and 3p), consistent with J. Sun, Liu, et al. (2022), and the wave-1 trend and climatology are out of phase.

To confirm the dynamical link between the different trends detected during the different months, it is worth investigating interannual variability (Figure 4). The scatterplot of the normalized indices of the averaged Arctic 2 m temperature in December and the averaged Arctic stratospheric temperature in March (with opposite sign) is shown in Figure 4a. There is a weak positive and non-significant correlation between the two indices (Table 1). This weak connection is confirmed by regressing the 2 m temperature in December onto the polar vortex index in March over the full 1979–2022 period (Figure 4e). The resulting map exhibits significant large-scale anomalies over Eastern Canada (positive) and over Siberia (negative), but does not show significant anomalies in the Arctic, in particular near the Barents-Kara sea regions.

The importance of the Canadian and Siberian anomalies is evidenced by composites of strong and weak polar vortex in March during the more recent 2001–2022 period (red dots in Figure 4a) shown in Figures 4b–4d and 4f–4h. The composite with strong polar vortex contains nine years, six of them being marked by a Sudden Stratospheric Warming (SSW) in January (2004, 2006, 2009, 2013, 2019, 2021) following the Charlton and Polvani (2007) criterion. The composite shows a warm anomaly in eastern Canada and a cold anomaly over Eurasia in the preceding December (Figure 4b). In contrast, the composite with weak polar vortex in March does not contain any years with SSWs in January, but all include warmings (SSWs or final warmings) in March following the Charlton and Polvani (2007) criterion (not shown). The latter composite shows a preceding cold anomaly over Canada, and a warm anomaly over Eurasia (Figure 4f) whose pattern is mainly in opposite phase with the wave-1 climatology (Figure 4g). To conclude, the anomalous composite of wave-1 temperature in December constructively (destructively) interferes with the wave-1 temperature climatology for strong (weak) polar vortex in March leading to positive (negative) upward wave-1 heat fluxes in December as shown in Figure 4d (Figure 4h). The

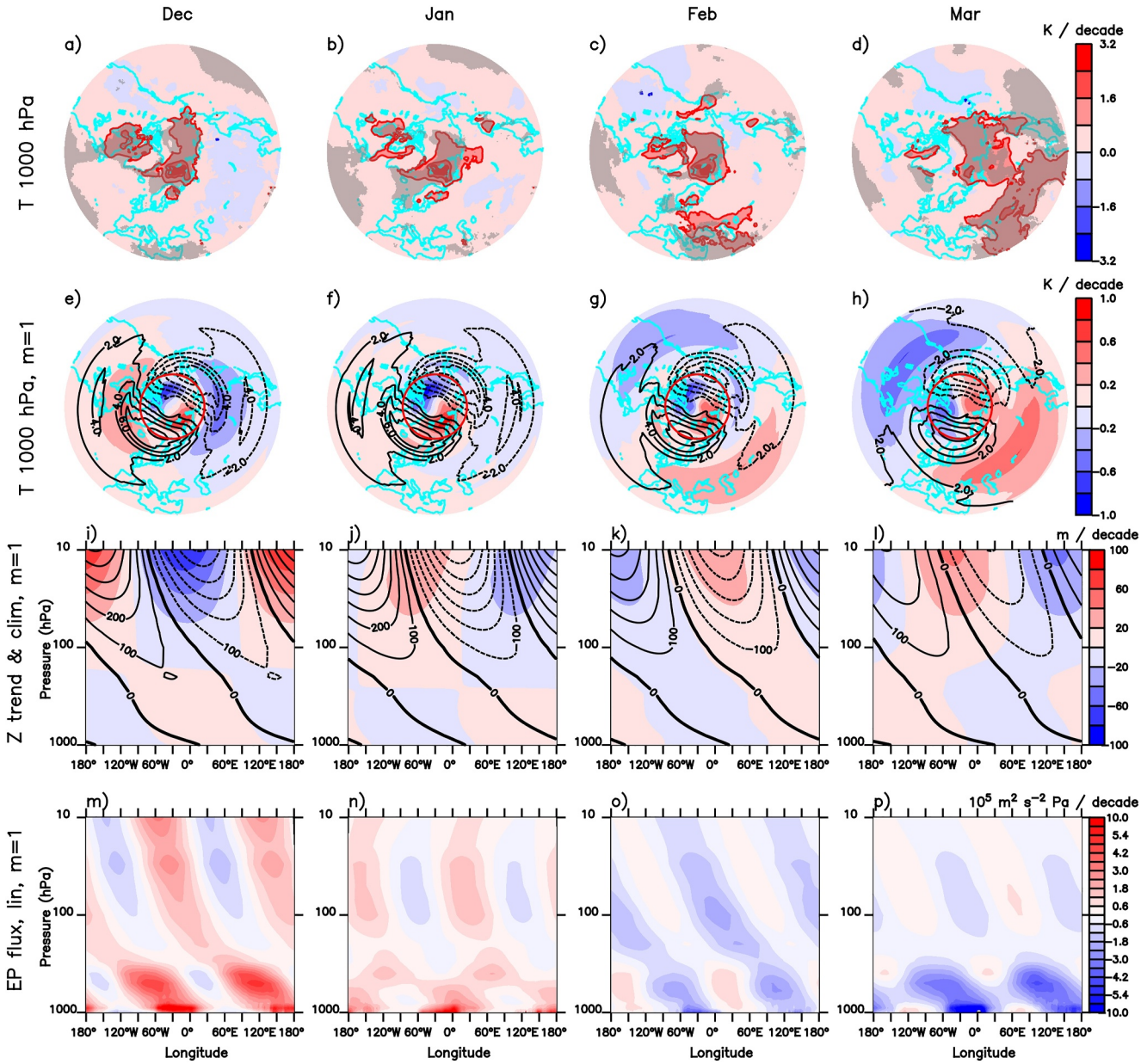

Figure 3. Trends from 1979 to 2022 for December to March (columns) of (a)–(d) 1,000 hPa temperature (shadings and red contours; interval: 0.8 K per decade), (e)–(h) 1,000 hPa temperature for wavenumber $m = 1$ (shadings; units: K per decade), (i)–(l) latitudinally averaged (50 N–70 N) geopotential height (shadings; units: m per decade) and (m)–(p) latitudinal average (50 N–70 N) of the linear vertical component of EP flux F_p for $m = 1$ (units: $10^5 m^2 s^{-2}$ Pa per decade). In (a)–(d), gray shading corresponds to significance larger than 99% (one-tailed test). In (e)–(h), black contours represent the 1,000 hPa temperature climatology for wavenumber $m = 1$ (interval: 2 K) and the red circle denotes the 70°N latitude. In (i)–(l), black contours represent the latitudinally averaged (50 N–70 N) geopotential height climatology for wavenumber $m = 1$ (interval: 100 m). Data: ERA5 at monthly time scales.

time-lag composites for strong (weak) SPV in March follow a chain of events similar to the trends with same (opposite) sign anomalies (see also Figures S6 and S7 in Supporting Information S1).

The correlation between wave-1 eddy heat fluxes at 100 hPa in December and the stratospheric polar vortex index in March is equal to 0.60 during the recent 2001–2022 period and 0.45 over the full 1979–2022 period, both correlations being statistically significant at the 99% level (see Table 1). We also compute three additional indexes in December, one based on the average of the 2 m temperature over Eastern Canada, another based on the average of the 2 m temperature over Eurasia and a third one by taking the differences between these two averaged temperatures (see red boxes in Figure 4e). The correlations over the full 1979–2022 period between these indexes

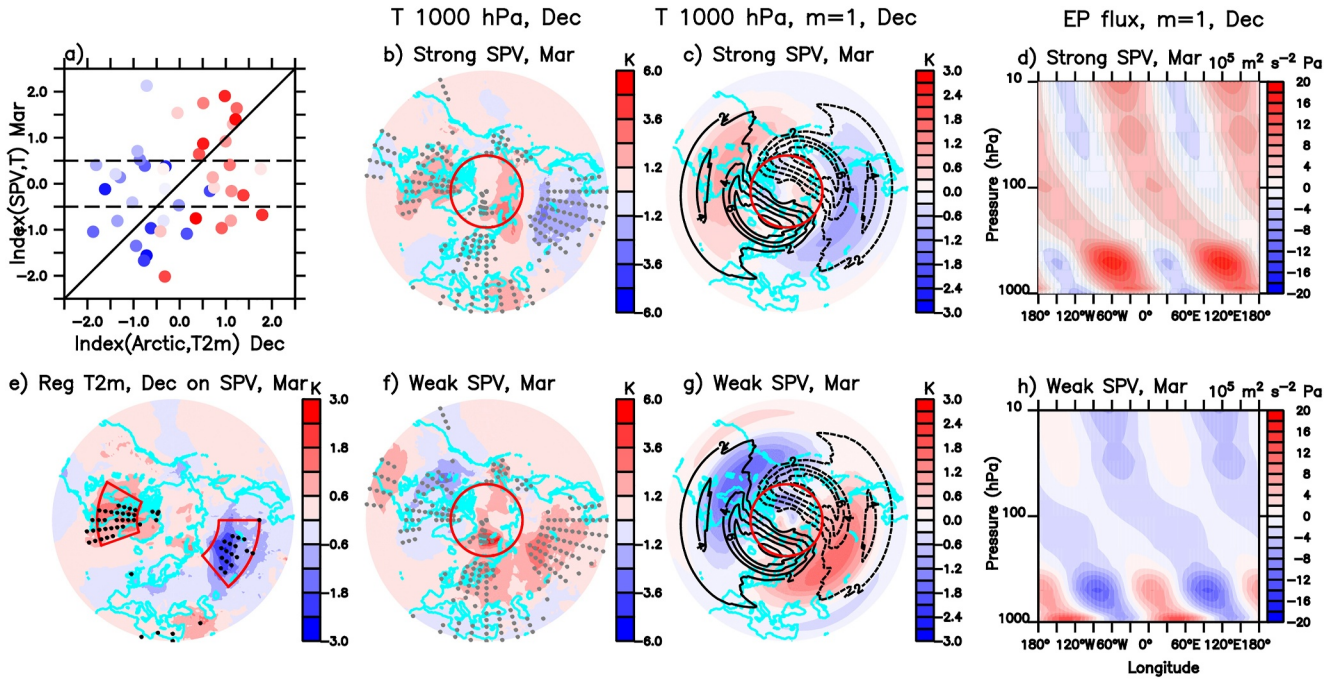

Figure 4. (a) Scatterplot of two normalized indices: the December 2 m temperature anomaly averaged between 70°N and 90°N (denoted as Index (Arctic, T2m)) and zero minus the March temperature anomaly averaged between 10 hPa and 50 hPa and between 70°N and 90°N (denoted as Index (SPV, T)). Blue (red) dots correspond to the 1979–2000 (2001–2022) period with the darker blue (red) dots corresponding to the oldest (newest) years of that period. Anomaly composites for (b), (c), (d) strong polar vortex (Index (SPV, T) in March greater than 0.5 standard deviations) and (f), (g), (h) weak polar vortex (Index (SPV, T) in March smaller than −0.5 standard deviations) during the recent period 2001–2022: (b), (f) anomalous 1,000 hPa temperature, gray dots representing regions where panels (b) and (f) are significantly distinct at the 99% confidence level following a two-sample two-tailed *t*-test, (c), (g) anomalous wave-1 1,000 hPa temperature (shadings) and climatological wave-1 1,000 hPa temperature (black contours; interval: 2 K), (d), (h) anomalous vertical component of Eliassen-Palm flux F_p averaged between 50°N and 70°N. The strong polar vortex composite in March is based on the following years: 2004, 2006, 2009, 2011, 2013, 2015, 2019, 2020, 2021 while the weak polar polar vortex composite in March contains the following years: 2005, 2008, 2014, 2016, 2018, 2022. (e) Regression of December 2 m temperature on Index (SPV, T) in March. The red boxes over Canada and Eurasia are used to compute indexes whose correlations with Index (SPV, T) are shown in Table 1. Data: ERA5 at monthly time scales.

and that of the stratospheric polar vortex in March are 0.47, −0.45 and 0.57, which are significant at 99% confidence level. This shows that it is not the intensity of the Arctic warming in December that matters for the strength of the polar vortex in March but rather the opposite-signed temperature anomalies over Eastern Canada and Siberia and their projection onto wave-1 climatology.

Table 1
Correlation Coefficients Between Different Indices in December (Vertical) and March (Horizontal)

(1979–2022) (1979–2000) (2001–2022)	Index (SPV, T) March	Index (SPV, NAM) March
Temperature 2 m Arctic Dec	0.26 –0.06 0.20	0.15 –0.12 0.14
Heat fluxes 100 hPa $m = 1$ Dec	**0.45** 0.29 **0.60**	**0.44** 0.33 **0.51**
Temperature 2 m Canada Dec	**0.47** 0.26 **0.50**	**0.43** 0.26 **0.51**
Temperature 2 m Eurasia Dec	**–0.45** –0.32 **–0.48**	–0.34 –0.28 –0.35
Temperature 2 m Canada-Eurasia Dec	**0.57** 0.44 **0.57**	**0.48** **0.40** **0.49**

Note. December indices are the 2 m temperature averaged in the Arctic (70°N-90°N) and the 100 hPa heat fluxes averaged between 50°N and 80°N for wavenumber 1. The two March indices correspond to two estimations of the stratospheric polar vortex intensity: one is equal to zero minus the temperature averaged between 10 and 50 hPa over the Arctic (70°N-90°N) and denoted as Index (SPV, T) and the other is the 10 hPa NAM index and denoted as Index (SPV, NAM). Black, blue and red correspond to the 1979–2022, 1979–2000 and 2001–2022 periods, respectively. Bold correlations are significant at 99% for a one-tailed test.

4. Conclusion and Discussion

Trends computed during the 1979–2022 period suggest that the following successive events in troposphere-stratosphere interaction occurred more often in the two latest decades. The chain of events starts with anomalous upward wave propagation for wavenumber 1 in December that leads to a deceleration of the SPV in January. This deceleration prevents tropospheric waves from propagating into the stratosphere in February, as found after SSW events (Hitchcock & Haynes, 2016), and supports a new acceleration of the SPV in March. The NAM increase in the stratosphere tends to favor a NAM signal of the same sign in the troposphere (Baldwin & Dunkerton, 2001). The dynamical link between the opposite January and March trends, particularly obvious during the recent 2018–2019 and 2020–2021 winters, is supported by the findings of Hauchecorne et al. (2022) who showed a strong anticorrelation between the SPV intensities at 2–3 month lags, in particular between January and March.

However, the trends are only weakly statistically significant because of strong interannual variability. Some recent winters, such as 2015–2016 or 2021–2022, were characterized by opposite signed patterns, while others do not fully project onto the trend scenario. We showed that recent winters with strong (weak) SPV in March are preceded by more (less) upward wave-1 propagation in December than usual due to constructive (destructive) interference of the wave-1 anomaly with the wave-1 climatology. This constructive (destructive) interference in December is associated with anomalous warming (cooling) over Eastern Canada and anomalous cooling (warming) over Eurasia. The connection is supported by a positive and highly significant correlation between the SPV intensity in March and the difference in averaged temperature between Eastern Canada and Siberia in December. This link does not necessarily mean that surface temperature anomalies in December drive the SPV fluctuations during the subsequent months. Our results rather show that wave-1 tropospheric anomalies in December trigger the SPV fluctuations and surface anomalies could be just the signature of those tropospheric anomalies.

These results show a potential for predictive skill of the March SPV intensity from the knowledge of the December surface temperature patterns between Eastern Canada and Siberia, rather than from the December Arctic temperature. We show that the Barents-Kara seas temperature, strong and positive across the latest period of data, is not a good predictor for the March SPV. This is to be contrasted with the findings of J. Sun, Liu, et al. (2022) who showed the influence of Barents-Kara sea ice anomalies in winter on extreme Eurasian heat waves in spring.

Following the above results, one may wonder if there are changes in the behavior of final stratospheric warmings (FSWs). Although, as already mentioned by Hauchecorne et al. (2022), no clear trend in the dates of FSWs is detected, the latest period (2001–2022) contains 15 late FSW and 7 early FSW while the oldest period (1979–2000) contains 10 late FSW and 12 early FSW, following the definition of FSW by Butler and Domeisen (2021). There is thus a tendency for later FSWs in the most recent period. However, since the correlation between the dates of FSWs and the NAM in March is only 0.3 over the whole period, the link between FSW and the trends in the coupled stratospheric-tropospheric system is not straight-forward.

One may also wonder what is the impact of SSW events on the weakening trend of the SPV in January and in our statistics in general. Since the earliest period (1979–2000) contains 2 SSWs and the latest period (2001–2022) 7 SSWs in January (not shown), this change in frequency certainly contributes to the general weakening trend of the SPV during that month. However, the correlations of the surface temperature indices with the SPV index (Table 1) do not change much when removing years with SSWs in January (not shown). Given the strong decadal variability in SSW occurrence (Domeisen, 2019; Reichler et al., 2012) and the limited number of SSWs events, the role of SSWs in the chain of events between mid-winter and early spring highlighted in the present paper needs further investigation.

One reason for the higher significance in the March trends with respect to the mid-winter trends lies in the fact that, although the intensity of the two stratospheric temperature trends is comparable, the January standard deviation is higher. An additional explanation could be related to positive feedbacks of ozone loss in early spring onto the intensity of the SPV (Friedel et al., 2022). Indeed, the presence of a strong SPV in early spring is accompanied by strong ozone loss due to less ozone transport from the tropics and enhanced springtime destruction of ozone favored by cold Arctic stratospheric conditions (Lawrence et al., 2020; Oehrlein et al., 2020).

The lack of ozone inside the vortex leads to less solar absorption that reinforces the cold stratospheric temperatures and hence the SPV strength.

Emerging observational evidence of mid-to-high latitude surface warming patterns modulating stratospheric variability (here and in Hamouda et al. (2024)) requires further investigation through tailored model experiments. Based on our results and those of J. Sun, Liu, et al. (2022), we also encourage future studies to investigate the predictive role played by mid-winter eddy heat fluxes and large-scale near-surface temperature anomalies on early spring stratospheric and tropospheric circulations. Following the same approach as in Butler et al. (2016) and Portal et al. (2022), it would be worth investigating the skill of seasonal forecast models initialized in mid-winter in predicting the SPV in early spring. In particular, the ability of the models to represent alternations in sign in eddy heat fluxes at 100 hPa and SPV intensities with 2–3 months lag would be of particular interest.

Data Availability Statement

ERA5 reanalysis data is described in Hersbach et al. (2020) is available from the Copernicus Climate Data Store: https://cds.climate.copernicus.eu (Hersbach et al., 2023).

MERRA-2 reanalysis data is described in Gelaro et al. (2017) and available via Global Modeling and Assimilation Office, MERRA-2 inst3_3d_asm_Np: 3d, 3 Hourly, Instantaneous, Pressure-Level, Assimilation, Assimilated Meteorological Fields V5.12.4, Greenbelt, MD, USA, Goddard Earth Sciences Data and Information Services Center (GES DISC). It can be accessed here: https://doi.org/10.5067/QBZ6MG944HW0.

Acknowledgments
GR was supported by ROADMAP (Role of ocean dynamics and Ocean-Atmosphere interactions in Driving cliMAte variations and future Projections of impact-relevant extreme events; https://jpi-climate.eu/project/roadmap/) project funded by Joint Programming Initiative "Connecting Climate Knowledge for Europe." Support from the Swiss National Science Foundation through project PP00P2_198896 to DD and through project IZCOZ0_205461 to AP are gratefully acknowledged.

References

Ayarzagüena, B., Charlton-Perez, A. J., Butler, A. H., Hitchcock, P., Simpson, I. R., Polvani, L. M., et al. (2020). Uncertainty in the response of sudden stratospheric warmings and stratosphere-troposphere coupling to quadrupled CO2 concentrations in CMIP6 models. *Journal of Geophysical Research: Atmospheres*, *125*(6), e2019JD032345. https://doi.org/10.1029/2019JD032345

Baldwin, M. P., & Dunkerton, T. J. (2001). Stratospheric harbingers of anomalous weather regimes. *Science*, *294*(5542), 581–584. https://doi.org/10.1126/science.1063315

Butler, A. H., Arribas, A., Athanassiadou, M., Baehr, J., Calvo, N., Charlton-Perez, A., et al. (2016). The climate-system historical forecast project: Do stratosphere-resolving models make better seasonal climate predictions in boreal winter? *Quarterly Journal of the Royal Meteorological Society*, *142*(696), 1413–1427. https://doi.org/10.1002/qj.2743

Butler, A. H., & Domeisen, D. I. V. (2021). The wave geometry of final stratospheric warming events. *Weather and Climate Dynamics*, *2*(2), 453–474. (Publisher: Copernicus GmbH). https://doi.org/10.5194/wcd-2-453-2021

Charlton, A. J., & Polvani, L. M. (2007). A new look at stratospheric sudden warmings. Part I: Climatology and modeling benchmarks. *Journal of Climate*, *20*(3), 449–469. https://doi.org/10.1175/JCLI3996.1

Cohen, J., Screen, J. A., Furtado, J. C., Barlow, M., Whittleston, D., Coumou, D., et al. (2014). Recent Arctic amplification and extreme mid-latitude weather. *Nature Geoscience*, *7*(9), 627–637. https://doi.org/10.1038/ngeo2234

Cohen, J., Zhang, X., Francis, J., Jung, T., Kwok, R., Overland, J., et al. (2020). Divergent consensuses on Arctic amplification influence on midlatitude severe winter weather. *Nature Climate Change*, *10*(1), 20–29. (Number: 1 Publisher: Nature Publishing Group). https://doi.org/10.1038/s41558-019-0662-y

Domeisen, D. I. (2019). Estimating the frequency of sudden stratospheric warming events from surface observations of the north atlantic oscillation. *Journal of Geophysical Research: Atmospheres*, *124*(6), 3180–3194. https://doi.org/10.1029/2018jd030077

Edmon, H. J., Hoskins, B. J., & McIntyre, M. E. (1980). Eliassen-palm cross sections for the troposphere. *Journal of the Atmospheric Sciences*, *37*(12), 2600–2616. https://doi.org/10.1175/1520-0469(1980)037⟨2600:EPCSFT⟩2.0.CO;2

Fletcher, C. G., & Kushner, P. J. (2011). The role of linear interference in the annular mode response to tropical SST forcing. *Journal of Climate*, *24*(3), 778–794. https://doi.org/10.1175/2010JCLI3735.1

Friedel, M., Chiodo, G., Stenke, A., Domeisen, D. I. V., Fueglistaler, S., Anet, J. G., & Peter, T. (2022). Springtime arctic ozone depletion forces northern hemisphere climate anomalies. *Nature Geoscience*, *15*(7), 541–547. https://doi.org/10.1038/s41561-022-00974-7

Gelaro, R., McCarty, W., Suárez, M. J., Todling, R., Molod, A., Takacs, L., et al. (2017). The Modern-Era Retrospective analysis for Research and Applications, version 2 (MERRA-2). *Journal of Climate*, *30*(14), 5419–5454. https://doi.org/10.1175/JCLI-D-16-0758.1

Gerber, E. P., & Martineau, P. (2018). Quantifying the variability of the annular modes: Reanalysis uncertainty vs. sampling uncertainty. *Atmospheric Chemistry and Physics*, *18*(23), 17099–17117. https://doi.org/10.5194/acp-18-17099-2018

Hamouda, M. E., Portal, A., & Pasquero, C. (2024). Polar vortex disruptions by high latitude ocean warming. *Geophysical Research Letters*, *51*(8), e2023GL107567. https://doi.org/10.1029/2023gl107567

Hauchecorne, A., Claud, C., Keckhut, P., & Mariaccia, A. (2022). Stratospheric Final Warmings fall into two categories with different evolution over the course of the year. *Communications Earth & Environment*, *3*(1), 1–5. https://doi.org/10.1038/s43247-021-00335-z

Hersbach, H., Bell, B., Berrisford, P., Biavati, G., Horányi, A., Muñoz Sabater, J., et al. (2023). Era5 hourly data on pressure levels from 1940 to present. *Copernicus Climate Change Service (C3S) Climate Data Store (CDS)*. https://doi.org/10.24381/cds.bd0915c6

Hersbach, H., Bell, B., Berrisford, P., Hirahara, S., Horányi, A., Muñoz-Sabater, J., et al. (2020). The ERA5 global reanalysis. *Quarterly Journal of the Royal Meteorological Society*, *146*(730), 1999–2049. https://doi.org/10.1002/qj.3803

Hitchcock, P., & Haynes, P. H. (2016). Stratospheric control of planetary waves. *Geophysical Research Letters*, *43*(22), 11–884. https://doi.org/10.1002/2016gl071372

Hoshi, K., Ukita, J., Honda, M., Nakamura, T., Yamazaki, K., Miyoshi, Y., & Jaiser, R. (2019). Weak stratospheric polar vortex events modulated by the Arctic seasea-ice loss. *Journal of Geophysical Research: Atmospheres*, *124*(2), 858–869. https://doi.org/10.1029/2018JD029222

Hu, D., Guan, Z., Tian, W., & Ren, R. (2018). Recent strengthening of the stratospheric Arctic vortex response to warming in the central North Pacific. *Nature Communications*, *9*(1), 1697. https://doi.org/10.1038/s41467-018-04138-3

Hu, D., Guo, Y., & Guan, Z. (2019). Recent weakening in the stratospheric planetary wave intensity in early winter. *Geophysical Research Letters*, *46*(7), 3953–3962. https://doi.org/10.1029/2019GL082113

Karpechko, A. Y., Afargan-Gerstman, H., Butler, A. H., Domeisen, D. I., Kretschmer, M., Lawrence, Z., et al. (2022). Northern hemisphere stratosphere-troposphere circulation change in CMIP6 models: 1. Inter-Model spread and scenario sensitivity. *Journal of Geophysical Research: Atmospheres*, *127*(18), e2022JD036992. https://doi.org/10.1029/2022jd036992

Karpechko, A. Y., Wu, Z., Simpson, I. R., Kretschmer, M., Afargan-Gerstman, H., Butler, A. H., et al. (2024). Northern hemisphere stratosphere-troposphere circulation change in CMIP6 models. Part 2: Mechanisms and Sources of the Spread. *Journal of Geophysical Research: Atmospheres*, *129*(13). https://doi.org/10.1029/2024JD040823

Kim, B.-M., Son, S.-W., Min, S.-K., Jeong, J.-H., Kim, S.-J., Zhang, X., et al. (2014). Weakening of the stratospheric polar vortex by Arctic sea-ice loss. *Nature Communications*, *5*(1), 4646. https://doi.org/10.1038/ncomms5646

Kretschmer, M., Zappa, G., & Shepherd, T. G. (2020). The role of Barents–Kara sea ice loss in projected polar vortex changes. *Weather and Climate Dynamics*, *1*(2), 715–730. (Publisher: Copernicus GmbH). https://doi.org/10.5194/wcd-1-715-2020

Lawrence, Z. D., Perlwitz, J., Butler, A. H., Manney, G. L., Newman, P. A., Lee, S. H., & Nash, E. R. (2020). The remarkably strong arctic stratospheric polar vortex of winter 2020: Links to record-breaking arctic oscillation and ozone loss. *Journal of Geophysical Research: Atmospheres*, *125*(22), e2020JD033271. https://doi.org/10.1029/2020JD033271

Liang, Y.-C., Kwon, Y.-O., Frankignoul, C., Gastineau, G., Smith, K. L., Polvani, L. M., et al. (2023). The weakening of the stratospheric polar vortex and the subsequent surface impacts as consequences to Arctic sea ice loss. *Journal of Climate*, *37*(1), 309–333. https://doi.org/10.1175/JCLI-D-23-0128.1

Long, C. S., Fujiwara, M., Davis, S., Mitchell, D. M., & Wright, C. J. (2017). Climatology and interannual variability of dynamic variables in multiple reanalyses evaluated by the SPARC Reanalysis Intercomparison Project (S-RIP). *Atmospheric Chemistry and Physics*, *17*(23), 14593–14629. https://doi.org/10.5194/acp-17-14593-2017

Oehrlein, J., Chiodo, G., & Polvani, L. M. (2020). The effect of interactive ozone chemistry on weak and strong stratospheric polar vortex events. *Atmospheric Chemistry and Physics*, *20*(17), 10531–10544. https://doi.org/10.5194/acp-20-10531-2020

Overland, J. E., Wood, K. R., & Wang, M. (2011). Warm Arctic—Cold continents: Climate impacts of the newly open Arctic sea. *Polar Research*, *30*(1), 15787. https://doi.org/10.3402/polar.v30i0.15787

Peings, Y. (2019). Ural blocking as a driver of early-winter stratospheric warmings. *Geophysical Research Letters*, *46*(10), 5460–5468. https://doi.org/10.1029/2019GL082097

Peings, Y., Davini, P., & Magnusdottir, G. (2023). Impact of ural blocking on early winter climate variability under different Barents-Kara sea ice conditions. *Journal of Geophysical Research: Atmospheres*, *128*(6), e2022JD036994. https://doi.org/10.1029/2022JD036994

Portal, A., Ruggieri, P., Palmeiro, F. M., García-Serrano, J., Domeisen, D. I. V., & Gualdi, S. (2022). Seasonal prediction of the boreal winter stratosphere. *Climate Dynamics*, *58*(7), 2109–2130. https://doi.org/10.1007/s00382-021-05787-9

Reichler, T., Kim, J., Manzini, E., & Kröger, J. (2012). A stratospheric connection to atlantic climate variability. *Nature Geoscience*, *5*(11), 783–787. https://doi.org/10.1038/ngeo1586

Ruggieri, P., Kucharski, F., Buizza, R., & Ambaum, M. H. P. (2017). The transient atmospheric response to a reduction of sea-ice cover in the Barents and Kara Seas. *Quarterly Journal of the Royal Meteorological Society*, *143*(704), 1632–1640. https://doi.org/10.1002/qj.3034

Rupp, P., Spaeth, J., Garny, H., & Birner, T. (2023). Enhanced polar vortex predictability following sudden stratospheric warming events. *Geophysical Research Letters*, *50*(17), e2023GL104057. https://doi.org/10.1029/2023GL104057

Santer, B. D., Wigley, T. M. L., Boyle, J. S., Gaffen, D. J., Hnilo, J. J., Nychka, D., et al. (2000). Statistical significance of trends and trend differences in layer-average atmospheric temperature time series. *Journal of Geophysical Research*, *105*(D6), 7337–7356. https://doi.org/10.1029/1999JD901105

Screen, J. A. (2017). Simulated atmospheric response to regional and pan-arctic sea ice loss. *Journal of Climate*, *30*(11), 3945–3962. https://doi.org/10.1175/JCLI-D-16-0197.1

Seviour, W. J. M. (2017). Weakening and shift of the Arctic stratospheric polar vortex: Internal variability or forced response? *Geophysical Research Letters*, *44*(7), 3365–3373. https://doi.org/10.1002/2017GL073071

Smith, K. L., & Kushner, P. J. (2012). Linear interference and the initiation of extratropical stratosphere-troposphere interactions. *Journal of Geophysical Research*, *117*(D13). https://doi.org/10.1029/2012JD017587

SPARC. (2022). In M. Fujiwara, G. L. Manney, L. J. Gray, & J. S. Wright (Eds.), *SPARC reanalysis intercomparison project (S-rip) final report*. (No. 10). https://doi.org/10.17874/800dee57d13

Sun, J., Liu, S., Cohen, J., & Yu, S. (2022). Influence and prediction value of Arctic sea ice for spring Eurasian extreme heat events. *Communications Earth & Environment*, *3*(1), 1–8. https://doi.org/10.1038/s43247-022-00503-9

Sun, L., Deser, C., Polvani, L., & Tomas, R. (2014). Influence of projected Arctic sea ice loss on polar stratospheric ozone and circulation in spring. *Environmental Research Letters*, *9*(8), 084016. https://doi.org/10.1088/1748-9326/9/8/084016

Sun, L., Deser, C., Simpson, I., & Sigmond, M. (2022). Uncertainty in the winter tropospheric response to Arctic sea ice loss: The role of stratospheric polar vortex internal variability. *Journal of Climate*, *35*(10), 3109–3130. (Publisher: American Meteorological Society Section: Journal of Climate). https://doi.org/10.1175/JCLI-D-21-0543.1

Sun, L., Deser, C., & Tomas, R. A. (2015). Mechanisms of stratospheric and tropospheric circulation response to projected Arctic sea ice loss. *Journal of Climate*, *28*(19), 7824–7845. Retrieved from https://doi.org/10.1175/JCLI-D-15-0169.1

Sun, L., Perlwitz, J., & Hoerling, M. (2016). What caused the recent "Warm Arctic, Cold Continents" trend pattern in winter temperatures? *Geophysical Research Letters*, *43*(10), 5345–5352. https://doi.org/10.1002/2016GL069024

Zhang, J., Tian, W., Chipperfield, M. P., Xie, F., & Huang, J. (2016). Persistent shift of the Arctic polar vortex towards the Eurasian continent in recent decades. *Nature Climate Change*, *6*(12), 1094–1099. (Publisher: Nature Publishing Group). https://doi.org/10.1038/nclimate3136